

Large-Scale Vertical and Horizontal Circulation in the North Atlantic Ocean

RICK LUMPKIN

Cooperative Institute for Marine and Atmospheric Studies, University of Miami, Miami, Florida

KEVIN SPEER

Department of Oceanography, The Florida State University, Tallahassee, Florida

(Manuscript received 4 March 2002, in final form 25 February 2003)

ABSTRACT

Observations of large-scale hydrography, air–sea forcing, and regional circulation from numerous studies are combined by inverse methods to determine the basin-scale circulation, average diapycnal mixing, and adjustments to air–sea forcing of the North Atlantic Ocean. Dense overflows through the Denmark Strait and Faroe Bank channels are explicitly included and are associated with strong vertical and lateral circulation and mixing. These processes in the far northern Atlantic play a fundamental role in the meridional overturning circulation for the entire ocean, accompanied by an upper cell of mode-water and intermediate-water circulation. The two cells converge roughly at the mean depth of the midocean ridge crest. The Labrador Sea Water layer lies within this convergence. South of the overflow region, model-derived mean diapycnal diffusivities are $O(10^{-5} \text{ m}^2 \text{ s}^{-1})$ or smaller at the base of the thermocline, and diapycnal advection is driven primarily by air–sea transformation on outcropping layers.

1. Introduction

The meridional circulation in the North Atlantic Ocean results from the interaction of several primary elements: western boundary currents (WBCs), the modification of northward-flowing Antarctic Intermediate and Bottom Waters (AAIW and AABW, respectively), and air–sea formation of subtropical and subpolar mode waters (STMW and SPMW, respectively) and Labrador Sea Water (LSW). Another primary element of meridional flow is the overflow of dense water from the Greenland–Iceland–Norwegian (GIN) Seas that ultimately forms the dense core of lower North Atlantic Deep Water (NADW). The overflow component has a long history of observation, and recent work (cf. Girton et al. 2001) goes much further toward a quantification of mean and variable outflow. But this component has not been incorporated into large-scale estimates of circulation except indirectly via tracer budgets (Smethie et al. 2000; Orsi et al. 2002) or as bulk transfers in coarse box models (Worthington 1976; McCartney and Talley 1982; McCartney 1992; Schmitz and McCartney 1993; Dickson and Brown 1994).

The replenishment of subtropical and subpolar mode waters is intimately tied to the strength of overturning, but also to diapycnal mixing, so concurrent estimates

of both flow and mixing are needed. How much mid-depth deep water is supplied from below via upwelling of dense Antarctic Bottom Water and overflow, as compared with the supply from above, via entrainment and convection in the mixed layer? Diapycnal mixing is necessary to form and support the NADW outflow, but how is it distributed?

We answer these questions with circulation estimates based on the box inverse model framework, which combines observations from hydrographic sections, current meters, and air–sea flux estimates. Unknown features of the circulation are inferred from prior property flux convergences. Absolute meridional transports are thus sensitive to boundary conditions at either end of the model. While many models have used net constraints set by the Pacific-to-Arctic Bering Strait exchange, no basin- or global-scale inverse model has taken advantage of the more detailed observations which can constrain mean exchanges between the North Atlantic and GIN Seas through the Greenland–Iceland–Scotland (GIS) choke point. Early models (Roemmich and Wunsch 1985; Rintoul and Wunsch 1991) focused on the tropical cell, subtropical gyre, and the development of the model framework, while more recent global models (Macdonald 1998, hereinafter M98; Ganachaud 1999, hereinafter G99) extend only to 48°N in the Atlantic—overturning across this latitude then becomes more sensitive to the choice of reference level since no explicit information closes the streamfunction farther north except bulk mass conservation. Because much of this transformation is

Corresponding author address: Rick Lumpkin, NOAA/AOML/PhOD, 4301 Rickenbacker Cswy., Miami, FL 33149-1097.
E-mail: Rick.Lumpkin@noaa.gov

driven by heat loss to the atmosphere, box models must also include air–sea fluxes if they are to attempt to distinguish this from other parts of the diapycnal transport.

Property transports in the ocean are naturally divided into components along and across constant density surfaces since the ocean is stratified and advection usually dominates mixing. While there has been a trend to convergent values of isopycnal transports (heat, for instance) across the principal transatlantic hydrographic lines, the diapycnal fluxes inferred from large-scale studies have been largely arbitrarily constrained or insignificant. More recent box inverse box calculations explicitly seek to resolve the diapycnal components as well as the isopycnal components by including air–sea fluxes of heat and fresh water and by building a degree of freedom into diapycnal fluxes that decouples them from ad hoc parameterizations (Sloyan and Rintoul 2001). Our approach in this study is similar, and we go to some length to represent in the prior circulation constraints derived by previous investigators. Various balances are then imposed to different degrees, that is, mass balance in layers, Ekman fluxes near the surface, and so on, with the goal of producing an estimate of the mean circulation consistent with the suite of observations. The reasonable existence of such a (record) mean is postulated and justified a posteriori by stable model solutions. Variability studies will be presented separately, but a sequence of inversions conducted with alternative repeats of two hydrographic lines demonstrates the robustness of the mean circulation derived for the World Ocean Circulation Experiment (WOCE) period.

In the following sections, we review diapycnal transformation by air–sea forcing and mixing (section two), describe construction of the box inverse model used in this study (section 3), discuss the results of the inversion (section 4), and make concluding remarks (section 5). In appendixes we present model-specific details: air–sea and river flux products used (appendix A), choices of prior model errors and unknown variances (appendix B), and the treatment of individual hydrographic sections (appendix C).

2. Transport and transformation in an isopycnal layer

In this study, isopycnal and diapycnal transports are inferred from property budgets within isopycnal oceanic layers. This formalism was developed from the isothermal construction of Walin (1982) and has been reviewed recently by Large and Nurser (2001).

Consider a layer of the ocean between isopycnal interfaces $\rho = \rho_o$ and $\rho = \rho_o + \Delta\rho$ within a domain bounded by bathymetry and a vertical control section running from one coastline to another. The layer volume ΔV changes according to

$$\begin{aligned} \partial_t \Delta V = & \Psi(\rho_o) - \Psi(\rho_o + \Delta\rho) + A(\rho_o) \\ & - A(\rho_o + \Delta\rho) + F_{\text{fw}}, \end{aligned} \quad (1)$$

where Ψ is the overturning streamfunction across the control section, $A(\rho_o)$ is the net diapycnal volume transport across the interface $\rho = \rho_o$ (defined positive toward increasing density), and F_{fw} is the freshwater flux ($P - E$) integrated over the layer’s outcrop area. The layer budget of a property with concentration C is

$$\begin{aligned} \partial_t (\langle C \rangle \Delta V) = & -\Delta\rho [\langle C \partial_\rho \Psi \rangle + \partial_\rho (\langle C \rangle A) + \partial_\rho D_c] \\ & + F_c + S_c, \end{aligned} \quad (2)$$

where $\langle \rangle$ is the layer or interface mean, $D_c(\rho_o)$ is the interior flux of C across the interface $\rho = \rho_o$ due to diffusion and to eddies (e.g., covariations of C and diapycnal advection across the interface), F_c is the air–sea input of the property at the layer outcrop, S_c is interior sources/sinks, and ∂_ρ is shorthand for the finite differential between the two interfaces. In the special case $C = \rho$, (2) becomes

$$\begin{aligned} \bar{\rho} \partial_t \Delta V = & \Delta\rho [-\bar{\rho} \partial_\rho (\Psi + A) - A(\bar{\rho}) - \partial_\rho D_\rho + F_\rho] \\ & + \rho_{\text{fw}} F_{\text{fw}}, \end{aligned} \quad (3)$$

where $\bar{\rho} = \rho_o + \Delta\rho/2$, interior sources of densification (e.g., cabbeling) have been neglected, and F_ρ is the transformation of density (buoyancy) due to air–sea fluxes of heat f_h and freshwater f_{fw} :

$$\begin{aligned} F_\rho = \int_{\text{outcrop}} \left[-\frac{g\alpha}{\bar{\rho}C_p} f_h(x, y, t) \right. \\ \left. + \frac{g\rho_{\text{fw}}\beta S}{\bar{\rho}(1-S)} f_{\text{fw}}(x, y, t) \right] dx dy \end{aligned} \quad (4)$$

(cf. Speer and Tziperman 1990). By taking (3) $-\bar{\rho} \times$ (1) and dropping the negligible terms associated with direct input by F_{fw} , one obtains the *transformation equation*

$$A = F_\rho - \partial_\rho D_\rho. \quad (5)$$

By substituting (5) into (1), one derives the *formation equation*

$$\partial_t \Delta V = -\Delta\rho \partial_\rho (\Psi + F_\rho - \partial_\rho D_\rho). \quad (6)$$

When the control section is a line of hydrographic casts, the streamfunction Ψ can be divided into four components,

$$\Psi = \Psi_{\text{Ek}} + \Psi_{\text{tw}} + \Psi_{\text{ref}} + \Psi', \quad (7)$$

representing the directly wind-driven transport, the thermal wind transport calculated with respect to an assumed reference level, the unknown reference component arising from nonzero transport on the reference level, and a bolus component that we shall neglect.

The terms F_ρ , Ψ_{Ek} , and Ψ_{tw} can be estimated from observations, leaving several unknowns in (6): the mass storage term (left-hand side), produced by interannual variations in diapycnal transformation and finite export time; the reference transport Ψ_{ref} ; and the mixing $\partial_\rho D_\rho$, which may be unequal to dispersion-based estimates at a point. Additional assumptions are needed to extract

TABLE 1. Hydrographic sections used in the control inversion. Dates are for the casts shown in Fig. 1, not for the entire cruise. Model parameters $|v_{\text{ref}}|_{\text{ap}}$ (cm s^{-1}) and T_{ap} (Sv) are defined in appendix B: (a) $T_{\text{ap}} = 0.25$ Sv for entire Iceland–Scotland ridge composite section, (b) $|v_{\text{ref}}|_{\text{ap}} = 30$ cm s^{-1} in the Straits of Florida. IFR: Iceland–Faroe Rise, FBC: Faroe Bank Channel, WTR: Wyville–Thompson Ridge, PB: Porcupine Bank.

Section	Chief scientist, research vessel	Dates	$ v_{\text{ref}} _{\text{ap}}$	T_{ap}
AR18	S-A, Malmberg, <i>Sæmundsson</i>	7–8 Sep 1995	10	0.25
IFR (west)	Ó. Ástthórsson, <i>Sæmundsson</i>	13–14 Jun 1998	10	0.25 ^a
IFR (east)	<i>Heinason</i>	9–12 Jul 1987	10	0.25 ^a
FBC, WTR	<i>Heinason</i>	11–13 Jun 1986	10	0.25 ^a
Faroe Bank	<i>Challenger</i>	10–14 Jun 1988	10	0.25 ^a
AR7E/A1E	A. Sy, <i>Valdiva</i>	14–27 Sep 1992	5	0.5
AR19/A2	A. Sy, <i>Gauss</i>	8–25 Jul 1993	2	1
AR16/AR6	E. Hagen, <i>Humboldt</i>	20–22 Sep 1992	10	0.25
A5	G. Parrilla, <i>Hespérides</i>	19 Jul–15 Aug 1992	1 ^b	2
A8	T. Müller, <i>Meteor</i>	1 Apr–7 May 1994	1	2

an absolute Ψ across a given latitude. Two recent approaches are representative. Marsh (2000) calculated yearly streamfunctions from time-varying fields of F_{ρ} north of 15°N in the Atlantic, equal to Ψ at 15°N in the limit of zero storage and mixing. Speer (1997) also assumed zero storage and calculated a similar, but time-mean, F_{ρ} north of 11°S , along with Ψ_{EK} at this latitude. He used the 11°S *Oceanus* hydrographic section (Speer et al. 1996) to estimate Ψ_{tw} and adjusted $\Psi + F_{\rho}$ within an estimated error range to determine the *minimum* necessary mixing $\partial_{\rho}D_{\rho}$. Speer (1997) found that interior mixing was necessary to account for the export of dense NADW, while air–sea formation alone could account for the export at subtropical thermocline densities ($\sigma_{\theta} = 26.6\text{--}27.6$).

3. A box inverse model

In this study, we extend the analysis of Speer (1997) by incorporating several hydrographic sections to achieve gyre-scale resolution of diapycnal and isopycnal transport. Explicit air–sea forcing is calculated from the Comprehensive Ocean–Atmosphere Data Set (COADS) and National Centers for Environmental Prediction–National Center for Atmospheric Research (NCEP–NCAR) reanalysis products (appendix A). We seek adjustments to the prior (thermal wind plus Ekman) flow field consistent with property conservation in isopycnal layers. The statistical framework for solving this problem in the steady-state limit is the box inverse model (cf. Wunsch 1996).

Earlier studies have applied this framework to North Atlantic hydrographic sections (Wunsch 1984; Roemich and Wunsch 1985; Rintoul and Wunsch 1991; M98), including several of the WOCE sections used in this study (G99). However, none of these studies has applied a priori heat and freshwater fluxes at the air–sea interface of the North Atlantic. Instead, heat conservation is not enforced in outcropping layers, and the mass loss associated with $E - P$ is treated as an unknown. Although these models’ *net* heat transport divergences are consistent with integrated heat fluxes

(Ganachaud and Wunsch 2000), it is not clear if individual layer budgets are consistent. The freshwater fluxes inferred by these models are not consistent with the integrated $E - P$ loss of $O(0.5$ Sv) ($11^{\circ}\text{S}\text{--}24^{\circ}\text{N}$; G99), but this too can be enforced in the layer budgets. In addition to missing available information on the *direct* input of heat and freshwater, these inversions must solve for the diapycnal advective transport A as an unknown to *lowest order*. They do not use (5) to divide A into two components, the unknown interior mixing and the estimable air–sea density transformation F_{ρ} . In the North Atlantic, F_{ρ} reaches ~ 30 Sv ($\text{Sv} \equiv 10^6 \text{ m}^3 \text{ s}^{-1}$), converges water into subtropical and subpolar mode water densities and plays a dominant role in closing the upper limb of the overturning circulation (Schmitt et al. 1989; Speer and Tziperman 1990; Speer 1997; Marsh 2000). Although air–sea flux products contain errors due to bulk parameterization and sampling biases, the gyre-scale structure of F_{ρ} is robust to lowest order in the North Atlantic. Our model calculates explicit layer by layer adjustments to account for errors, thus producing a set of adjusted heat and freshwater fluxes consistent with continuity and hydrography.

Neglecting air–sea transformation is problematical where many layers outcrop, for example, in the subpolar Atlantic where cooling produces subpolar mode water and, at the extreme end of SPMW, Labrador Sea Water (McCartney and Talley 1982, 1984), which is exported southward at upper NADW densities. The box models of M98 and G99 circumvent this issue in the North Atlantic by choosing a nominal 48°N section as their northernmost boundary. However, in the absence of information north of 48°N , the overturning (and associated properties such as heat transport) becomes a stronger function of the prior thermal wind reference level and transport error bars are magnified (see section 3b). The best estimates of absolute transports must be based upon an integration of divergences from a well-constrained boundary, for example, the bathymetric choke point of the GIS ridges where extensive current observations (Ross 1984; Saunders 1990; Østerhus et al. 1999; Hansen et al. 1999; Garton et al. 2001; Price et al. 2001)

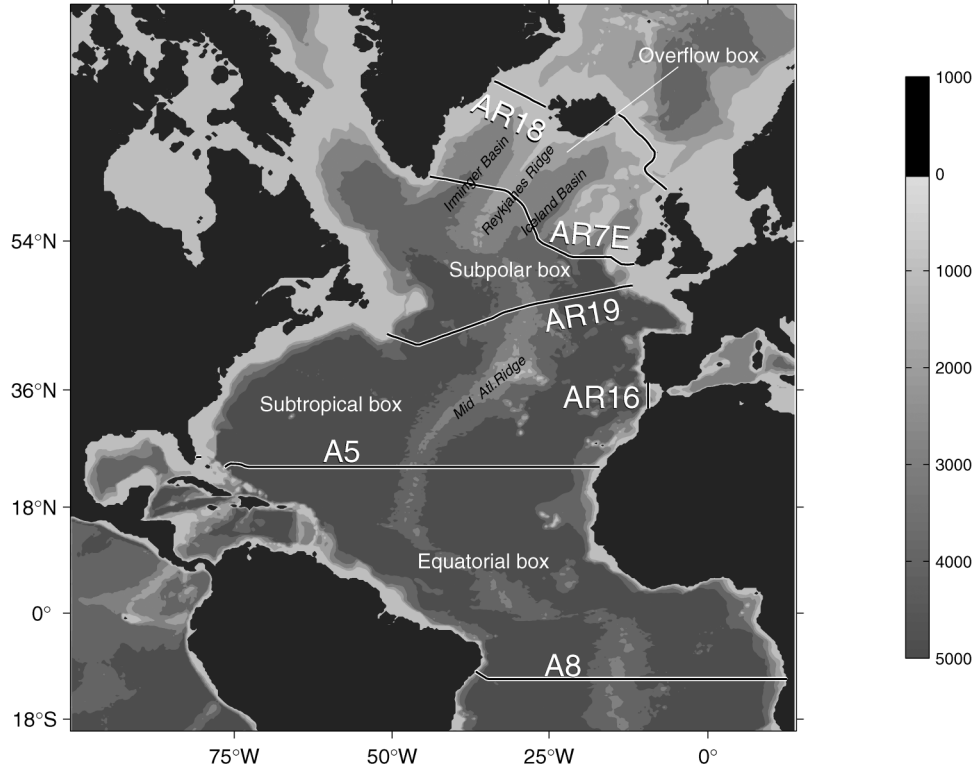


FIG. 1. Geometry of the box inverse model, superimposed on bathymetry (m).

constrain exchanges with the GIN Seas and Arctic Ocean (cf. Mauritzen 1996).

a. Model construction

Hydrographic sections (Table 1) are used to divide the North Atlantic into four boxes (Fig. 1). Each box is divided into 45 isopycnal layers separated by interfaces of constant neutral density γ^n (Jackett and McDougall 1997). These interfaces were defined such that the 35 densest layers contain equal volumes of the global ocean according to the SAC/Hamburg climatology (Gouretski and Jancke 1998). Increased density resolution at $\gamma^n < 26.5$ helps to resolve transformation of

outcropping water masses in the Tropics and subtropics. To facilitate presenting and discussing model results, we refer to blocks of layers (Table 2) illustrated in Fig. 2. Upper deep layers span the density range of Labrador Sea Water in the subpolar gyre, and include the high-salinity core of upper NADW passing southward across 11°S. Lower deep layers span the density range of lower NADW and intermediate Nordic Seas Overflow Water (NSOW) and are unventilated in the North Atlantic. Bottom layers include Antarctic Bottom Water and the densest NSOW.

The model solves conservation equations based on (2) and (5). In layer i bounded by hydrographic station pairs $j = 1, \dots, N$, these take the form

$$\sum_{j=1}^N \left[\Delta x_j \int_i C_j(v_{\text{ref},j} + b_j) dz + (1 + e^*) \Psi_{\text{Ek},ij} C_{j,10\text{m}} \right] + \bar{C}_{i-1} A_{i-1} - \bar{C}_i A_i + F_{c,i} + F_{c,i}^* + (\partial_\rho D_c)_{i-1} - (\partial_\rho D_c)_i \approx 0, \tag{8}$$

where Δx_j is the distance between station pair j , the vertical integral spans the pair-dependent thickness of layer i , $C_j(z)$ is the pair-averaged profile of property C , v_{ref} is a reference level adjustment to the prior thermal wind profile $b_j(z)$, e^* is a fractional adjustment to each section's Ekman transport, \bar{C}_i is the interface-averaged

value of C within the box, and F^* is an adjustment to the air-sea input of C . For mass conservation, $C = \rho$, $\partial_\rho D = 0$ (no diffusion of mass), and $F_c = \rho_{\text{fw}} F_{\text{fw}}$. For heat anomaly (thermal energy with respect to 0°C) conservation, $C = \rho \theta C_p$ and $F_c = F_h$. For salt anomaly conservation, $C = \rho(S - 35)/1000$ and $F_c = 0$. For all

TABLE 2. Blocks of isopycnal layers referred to in the text: “layers” indicates layer numbers in the inverse model, “ γ^n ” is the neutral density at the upper interface, “potential density” shows a corresponding value of σ at 48°N, and “water masses” within the blocks are indicated (see Fig. 2).

Name	Layers	γ^n	Potential density	Water masses
Surface (SFC)	1–7	Surface		
Thermocline (TC)	8–11	25.9	$\sigma_\theta = 26.0$	STMW
Intermediate (INT)	12–20	27.15	$\sigma_\theta = 27.10$	AAIW, MOW, SPMW, AW
Upper deep (UD)	21–24	27.88	$\sigma_{1.5} = 34.59$	LSW, NADW, NSOW
Lower deep (LD)	25–36	27.98	$\sigma_{2.5} = 39.16$	NADW, NSOW
Bottom (BOT)	37–45	28.12	$\sigma_4 = 45.89$	AABW, NSOW

property budgets, the diapycnal advection A is given by $A_i = (F_\rho + F_\rho^* - \partial_\rho D_\rho)_i$, where $(F_\rho + F_\rho^*)_i$ is calculated from adjusted heat and freshwater fluxes at the layer’s outcrops. Gauss–Markov estimation (Wunsch 1996) is used to solve for the unknowns: v_{ref} for each station pair, e^* for each hydrographic section, F_{fw}^* and F_h^* for outcropping layers in each box, and $\partial_\rho D$ for density, heat, and salt across each interface within each box. Details regarding prior unknown variances and model errors are given in appendix B. Within each box, the net (all layers) mass, heat, and salt were also conserved via explicit constraints. Additional section-dependent constraints, such as layer exchanges with the GIN Seas across the GIS ridges, were imposed upon the solution as documented in appendix C.

Both this model and that of Sloyan and Rintoul (2001, hereinafter SR01) have explicit air–sea forcing. How-

ever, the property budgets (8) are constructed differently. We assume that a property-independent diapycnal transport A advects all properties from one layer to another, as in G99; SR01 assumed an independent diapycnal transfer for each property. This distinction is somewhat arbitrary, however, because we include an additional property-dependent diffusive or eddy flux, unlike the property independent diffusivity of G99, and thus our equations contain the same degrees of freedom as those of SR01. A more fundamental distinction is that SR01 added the explicit interior (within box) Ekman diapycnal advection A_{Ek} to their budgets, yielding the prior diapycnal transport $A = F_\rho + A_{\text{Ek}}$. Their inversion simultaneously adjusted F_ρ and mixing, parameterized by an effective diapycnal velocity w^* . However, in the derivation of the volume budget (6), the net diapycnal advection A , which implicitly includes the in-

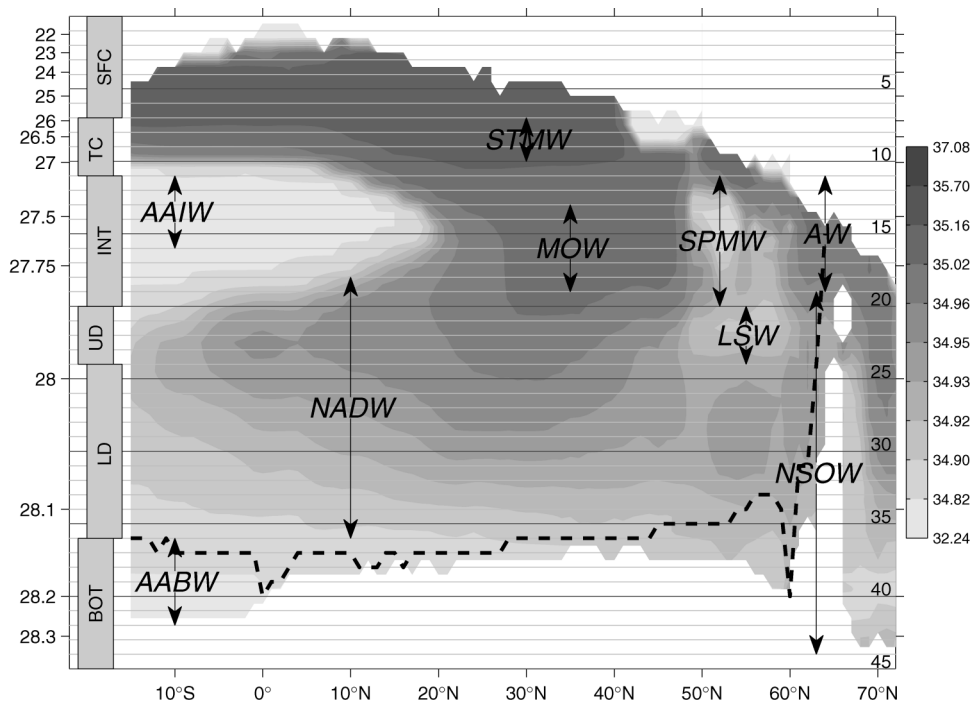


FIG. 2. Neutral density layers in the inverse model. Layers (numbered at right) are separated by interfaces of constant γ^n (left). Shading: zonally averaged salinity from SAC/Hamburg climatology. Black dashed line: densest water east of the Mid-Atlantic and Reykjanes Ridges. In addition to those defined in the text, labeled water masses are Mediterranean Outflow Water (MOW) and Atlantic Water (AW). Bars at left denote blocks of layers (see Table 2).

terior Ekman component, is replaced by $F_\rho - \partial_\rho D_\rho$. The additional explicit A_{Ek} term in SR01's volume budget must be combined with their w^* term to infer mixing $\partial_\rho D_\rho$. Thus, SR01 have found a solution from the prior choice $-\partial_\rho D_\rho = A_{\text{Ek}}$, $w^* = 0$, $A = F_\rho + A_{\text{Ek}}$, while we choose the minimal mixing prior $-\partial_\rho D_\rho = 0$, $A = F_\rho$. In oceanic layers where the primary balance is $A \sim A_{\text{Ek}} = F$; that is, where net transformation is dominated by a surface buoyancy flux consistent with the mean Ekman transport across isopycnals, their choice would inappropriately double the prior transformation and drive the solution toward spuriously large mixing. In oceanic layers where strong mixing is associated with A_{Ek} and F_ρ is relatively small, their prior choice would be more appropriate while ours would tend to produce minimal estimates of both A and the interior mixing. In summary, our construction reflects a prior choice that will tend to produce weaker overturning and less mixing than that of SR01 wherever it is applied, and can be considered a *minimum mixing* scheme.

b. Experimental inversions

In addition to the "control" inversion constructed as in Fig. 1, a number of experimental runs were conducted. Two of these were particularly revealing:

1) EFFECT OF INFORMATION NORTH OF 48°N

Previous large-scale box inversions (M98; G99) have used the 48°N section as their northern boundary. By including explicit hydrographic information farther north and requiring that the model be consistent with estimates of GIN Seas overflows and exchanges, our model is better able to constrain property transports and is less sensitive to the initial reference level choice at 48°N. To demonstrate this, we ran suite of two-box inversions, consisting of the equatorial and subtropical boxes (11°S–48°N). Bering Strait throughflow-derived constraints for net volume and salt (Wijffels et al. 1992) were applied at the 48°N northern boundary, and all else was identical to the control (four box) inversion including explicit air–sea forcing in the two boxes (not present in previous inversions). Because the two-box inversions lack information regarding subpolar air–sea forcing, exchanges with the GIN Seas and conservation in subpolar layers, their transports are less well constrained and more strongly dependent upon the initial reference level choice than those of the control inversion (Fig. 3). For very dense initial reference levels, the four-box inversion was not able to satisfy the constraints within the prior choices of the inversion; these results are not shown in Fig. 3.

The M98 and G99 inversions included hydrographic sections and continuity south of 11°S, not included in our control inversion. However, because there is no southern choke point comparable to the GIS ridges, nor South Atlantic outcropping and air–sea-driven trans-

formation comparable to the subpolar North Atlantic, this information does not affect transports across 11°S as dramatically as in Fig. 3. In an experimental inversion with an additional South Atlantic box (bounded to the south by the 30°–45°S line A11), overturning across 11°S had a maximum strength of 15.8 ± 2.1 Sv (16.4 ± 2.1 Sv in the control run) and the net transport across 11°S was 0.68 ± 0.10 PW (0.69 ± 0.10 PW control), not significantly different within the nearly identical error bars.

2) EFFECT OF HYDROGRAPHIC VARIABILITY

Recent analyses of hydrographic repeats at 48°N (Koltermann et al. 1999), 60°N (Bersch et al. 1999) and in the deep boundary current off Cape Farvel (Bacon 1998) have deduced significant variations in North Atlantic property transports. In the steady-state inversion of this study, these variations must be absorbed by model error terms or cancelled by adjustments to the initial level of no motion [e.g., 1000 m in Bacon (1998)]. To assess the impact of hydrographic variations upon the solution, we reran the model with the 16 possible combinations of four 48°N A2/AR19 repeats (1993, 1996, 1998, 1999) and four 60°N A1E/AR7E repeats (1991, 1992, 1995, 1996), everything else identical to the control run. The 16-ensemble-mean diapycnal transformation differs by less than one standard deviation from the control inversion in all layers (Fig. 4), demonstrating that, when given identical constraints for North Atlantic/GIN Seas exchanges, the model is able to produce a robust time-mean circulation via acceptable adjustments to the unknowns and absorption by model error terms. The inverse solution is altered more dramatically when one makes large changes to the boundary condition constraints, for example, by doubling or halving the overflow through the Denmark Strait channel. Observed changes in the overflow are smaller (Girton et al. 2001) but experimental runs such as these demonstrate the importance of choke-point observations for monitoring overturning variability.

4. North Atlantic circulation and transformation

The inversion was able to derive a set of unknowns within the range of prior variance (appendix B) which satisfied property conservation and additional, section-dependent constraints (appendix C) within specified prior model error. Neighboring solutions, in the sense of small adjustments to initial conditions, constraints, layer definitions, and model errors, were very similar and in this sense the result is considered stable. Figure 5 shows the adjusted air–sea density, heat, and freshwater inputs in each box derived by the model. In most layers the adjusted air–sea inputs are not significantly different than given by the University of Wisconsin—Milwaukee (UWM)/COADS or NCEP–NCAR reanalysis products, although they tend to match more closely the NCEP–

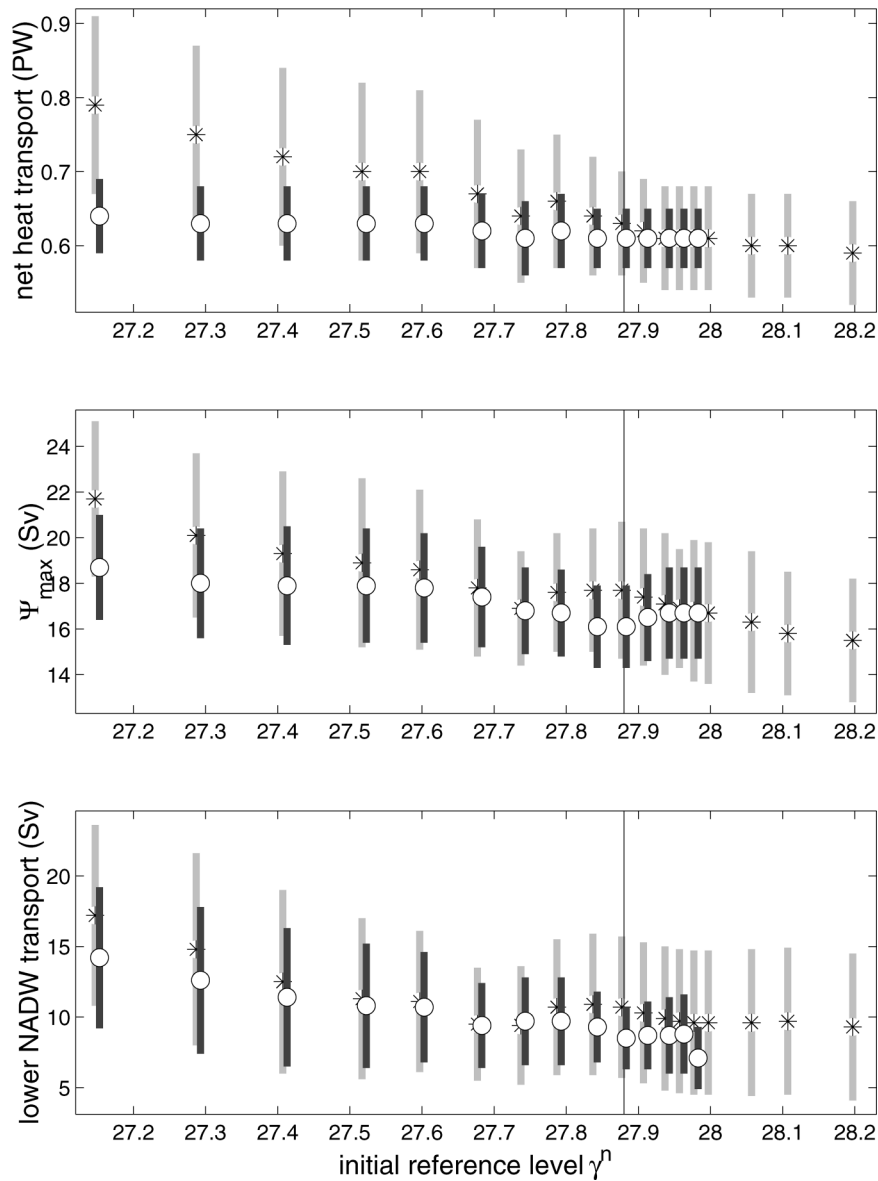


FIG. 3. (top) Net heat transport, (middle) overturning strength, and (bottom) southward transport of lower NADW across 48°N , as a function of thermal wind reference level (horizontal axis; black line marks the value used in the control inversion). Results from the four-box inversion are white bullets, with black standard error bars. Results from a two-box inversion (the equatorial and subtropical boxes) are asterisks, with gray standard error bars.

NCAR values. The interior mixing $\partial_{\rho}D$ is shown in Fig. 6, as a function of model layer (see Table 2). Figure 7 shows $\partial_{\rho}D_{\rho}$ converted to an effective diffusivity $\langle\kappa\rangle$ using layer mean values from the SAC/Hamburg climatology (Gouretski and Jancke 1998); error bars do not include uncertainties in these climatological values. Some very dense layers present in the hydrography do not exist in the climatology; for these, the volume was extrapolated and the error bars in Fig. 7 were magnified.

Net transports of volume, salt, and heat after inversion are given in Table 3. By construction, divergences in heat and volume transport are consistent with the ad-

justed air–sea heat and freshwater inputs. The equatorial box gains 0.41 ± 0.07 PW from the adjusted heat fluxes, while the subtropical, subpolar, and overflow boxes lose 0.37 ± 0.04 , 0.17 ± 0.03 and 0.14 ± 0.01 PW, respectively.

Figure 8 shows the distribution of volume transport in the model layers, integrated bottom to top (i.e., the overturning streamfunction Ψ). A schematic of the two-dimensional meridional overturning circulation, Fig. 9, is produced by linearly interpolating Ψ between the sections and extrapolation to zero north of the nominal 66°N overflow ridge sections. Because this schematic

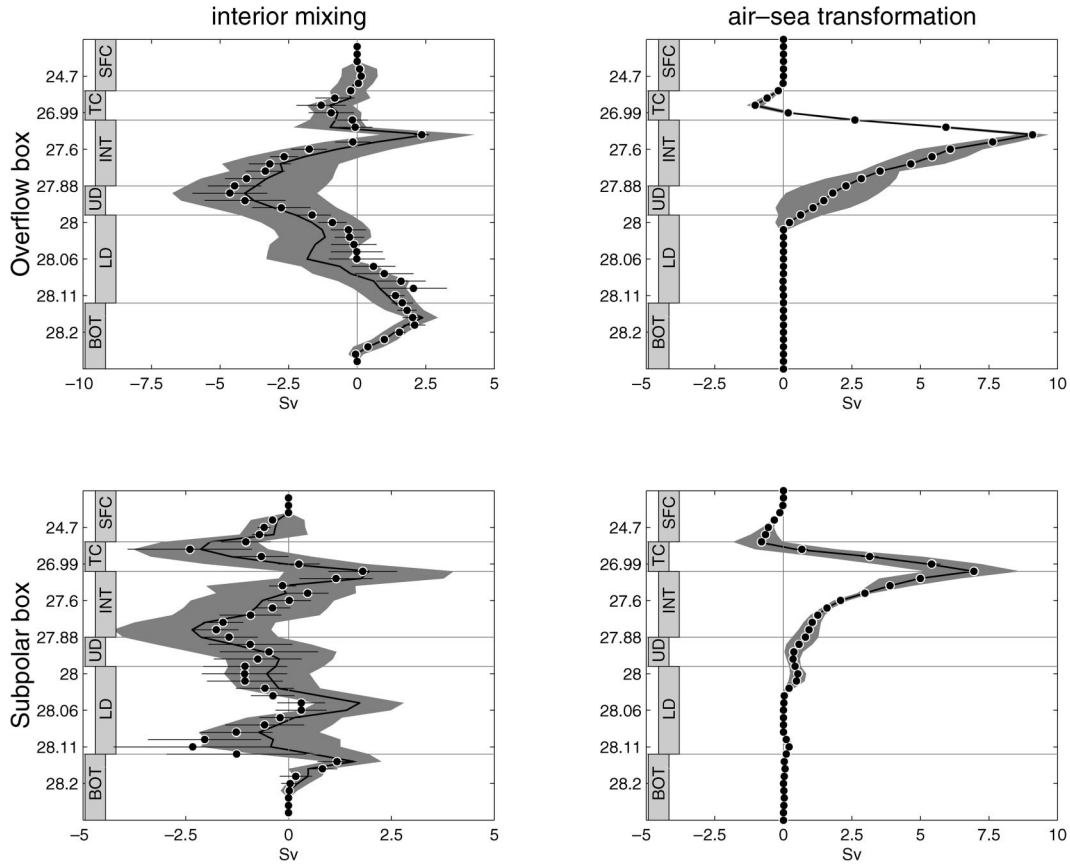


FIG. 4. (left) Interior and (right) air-sea diapycnal transformation in the (top) overflow and (bottom) subpolar boxes. Bullets indicate the ensemble mean of 16 inversions using combinations of repeat hydrographic lines at 48° and 60°N; horizontal lines show their standard deviations. The control inversion is a heavy black line, with the standard error shaded.

is presented in model layer (density) coordinates, diapycnal transformation is indicated by nonhorizontal streamlines. Figure 10 presents a top view of the circulation, showing separately the western boundary and interior components of the shallow (white) and deep (black) pathways.

In the remainder of this section, we compare the results of our inversion with those of M98 and G99, where the domains of these inversions overlap (11°S–48°N). We then discuss the pathways of isopycnal circulation and diapycnal transformation that define the three-dimensional circulation of the North Atlantic in our solution.

a. Comparison with previous inversions

Over the domain 11°S–48°N, our model circulation loses a net 0.3 ± 0.1 Sv to integrated $E - P - R$, consistent (by construction) with estimated air-sea fluxes and riverine input. In contrast, G99 gains 0.2 ± 0.2 Sv (M98 gains 0.05 Sv) over this domain, presumably affected by his prior choice of 0 Sv.

In the subtropical box, the gross features of the me-

ridional overturning circulation derived by our inverse model are similar to those of G99. The northward transport of 15.6 ± 1.3 Sv surface, thermocline, and intermediate water at 24°N and 48°N (16 ± 2 Sv in G99) is balanced by an equal southward transport of NADW at 48°N, increased slightly at 24°N by upwelling of 0.9 ± 2.1 Sv AABW (G99: 1 ± 1 Sv) within the subtropical box. There is no significant net exchange between the northward and southward overturning limbs within the subtropical box, as in G99 but unlike M98 in which a divergence of 6 Sv in the northward layers was fed by upwelling. The southward flow of NADW across 48°N is substantially less than M98's 25 ± 1 Sv, primarily in the layers $\gamma^\sigma > 28.12$ ($\theta < 2.0$) where our solution has 0.5 ± 1.0 Sv crossing 48°N, while M98 found 10 ± 1 Sv. As only 3.7 ± 0.3 overflows the GIS ridges at these extreme densities, and upwelling in the overflow box reduces this to 2.2 ± 0.6 Sv flowing past Cape Farvel (60°N), it is unclear what process could feed 10 Sv at these densities. The discrepancy with M98 may be due to temporal variability (pre-WOCE section in M98, WOCE here) or a bottom triangle problem in M98 (G99, pg. 118). In our solution, the deep western bound-

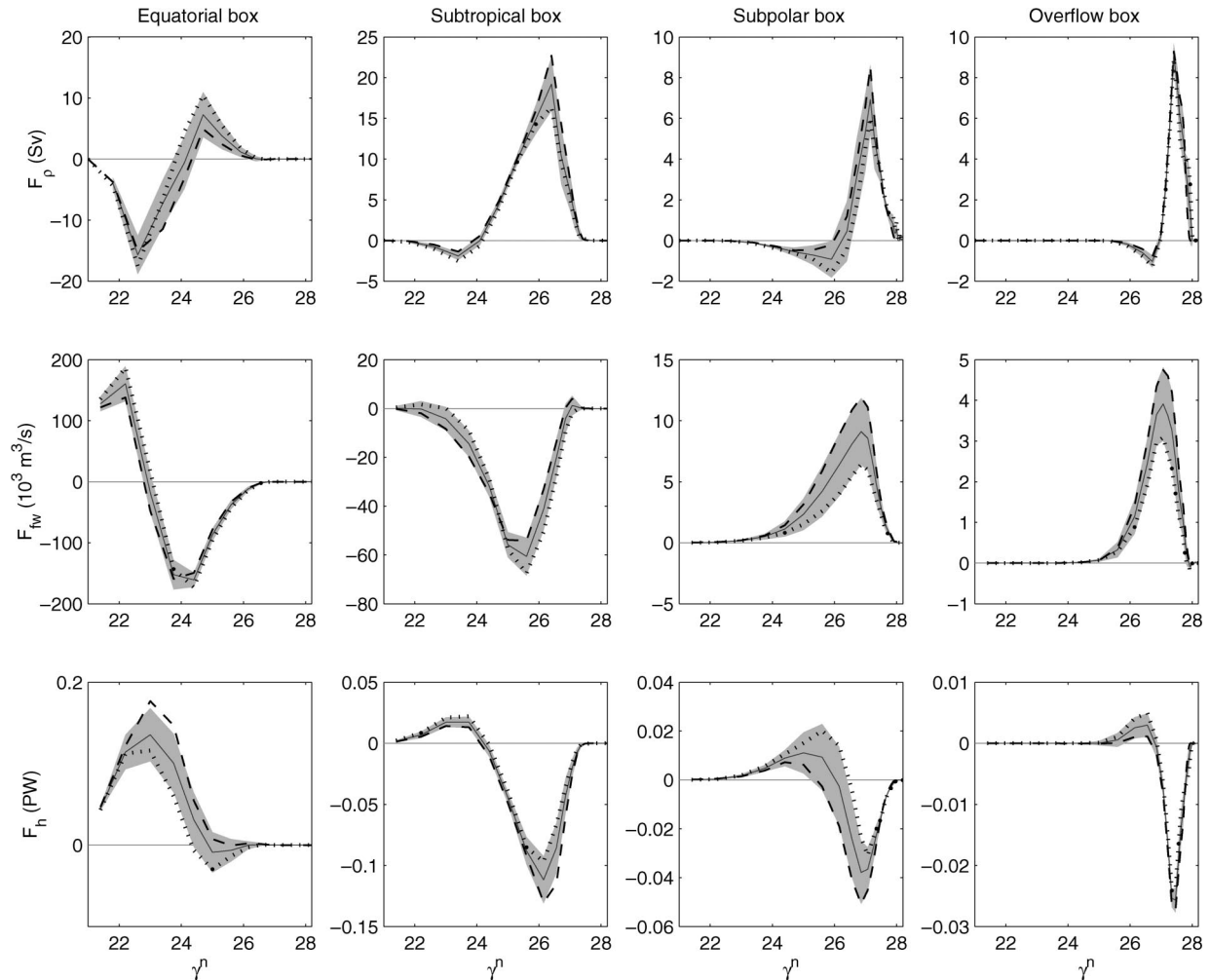


FIG. 5. Air-sea fluxes of (top) buoyancy, (middle) freshwater and (bottom) heat in each of the four boxes of the inverse model; shading is standard error. The buoyancy flux F_p is calculated from the freshwater and heat fluxes. Dashed lines: prior fluxes from UWM/COADS. Dotted lines: prior fluxes from NCEP-NCAR reanalysis. Positive F_p corresponds to a diapycnal advection toward greater density.

ary current (DWBC) is twice the strength of the northward deep interior flow. At 48°N our solution shows a 14 Sv deep cyclonic recirculation in the Newfoundland Basin (Fig. 10), not present in the McCartney (1992) or Schmitz and McCartney (1993) schemes but qualitatively similar to M98's 5 Sv recirculation. At 24°N , M98 found a southward transport of 19 ± 2 Sv NADW, similar to the 17.6 ± 2.7 Sv in our model and in earlier estimates (e.g., ~ 18 Sv, Wunsch and Grant 1982; 20 ± 5 Sv, Roemmich and Wunsch 1985). The primary difference between our results and those of G99 in the subtropical box is that transports in our solution are in general more tightly constrained because of the propagation of information from the subpolar gyre (see section 3b). Other major differences are that we resolve transport and transformation at densities lighter than $\gamma^n = 26.44$, where air-sea-driven advection must be balanced by significant heat and salt diffusion, and we do not find significantly nonzero downwelling in the upper

deep density range $27.92 < \gamma^n < 28.0$, present in G99. Last, our solution requires a different relative combination of salt and heat mixing in the thermocline layers (discussed below), which would not be accommodated by G99's property-independent diffusivity.

Within the equatorial box, our solution and M98, G99 find that 2–4 Sv of AABW is converted to lower deep densities, associated with a diffusivity of $O(10^{-3} \text{ m}^2 \text{ s}^{-1})$ (Fig. 7). This conversion increases the DWBC transport of NADW at 11°S from its value at 24°N . However, while both M98 and G99 show conversion of northward-flowing AAIW to southward-flowing NADW (5 Sv in M98, 2 Sv in G99) between 11°S and 24°N , we find negligible downwelling across the AAIW/NADW interface. As a consequence, we find a smaller transport of NADW across 11°S : 19.6 ± 2.4 Sv, as compared with 28 ± 1 in M98 and 23 ± 4 in G99. In the core NADW density range $27.5 \leq \gamma^n \leq 28.11$, Speer et al. (1996) inferred a southward transport of 14 Sv across

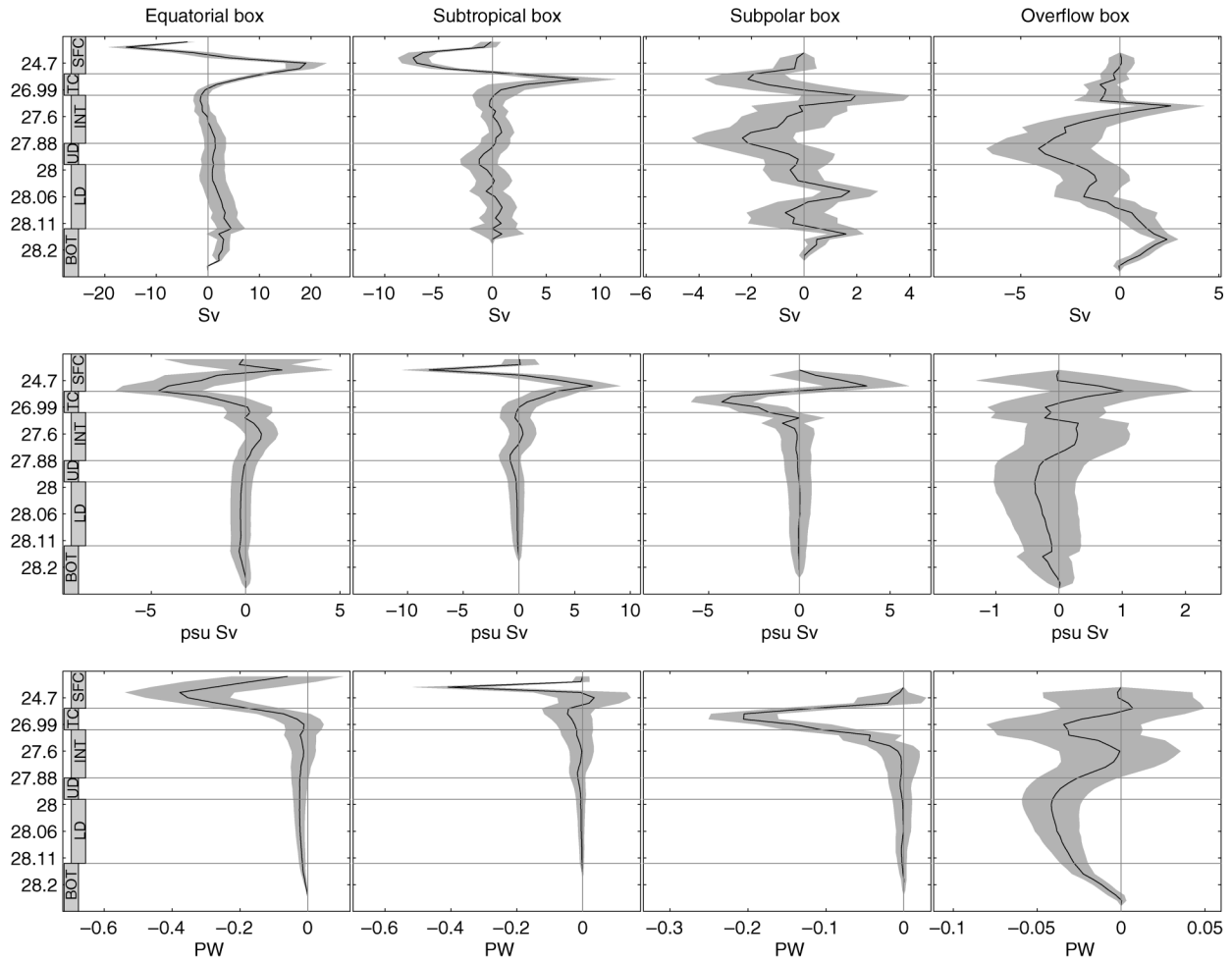


FIG. 6. Interior diapycnal transports of (top) volume and diffusive or eddy fluxes of (middle) salt anomaly and (bottom) heat anomaly in the four boxes; shading is standard error. Positive values are toward decreasing neutral density (upward).

11°S; our adjusted field carries 18.2 ± 2.5 Sv, comparable to G99's 20 ± 4 Sv in these layers. The upper, northward-flowing branch of the M98 and G99 solutions were stronger at surface densities, while ours is stronger at intermediate densities, yielding a smaller net heat transport across 11°S in our solution (0.69 ± 0.1 PW, vs 0.9 ± 0.4 PW in G99).

b. The three-dimensional North Atlantic circulation

The North Atlantic overturning circulation is fed by 16 Sv of surface to upper intermediate water ($\gamma^n < 27.6$) passing north across 11°S. This is carried primarily by the North Brazil Current, as the net interior (non-WBC) transport in these layers is 0.1 ± 4.1 Sv. Surface water absorbs 0.41 ± 0.07 PW from the atmosphere within the equatorial box, producing a strong buoyancy gain in the warm pool layers, which must be balanced by mixing (Niiler and Stevenson 1982). In the model solution, a 16 Sv mixing-driven downwelling opposes the air-sea-driven transformation across $\gamma^n = 22.6$. Down-

ward heat diffusion reaches a maximum of 0.4 PW in these layers (Fig. 6). At densities $\gamma^n = 23$ –24, the adjusted air–sea heat input is significantly smaller than the integrated UWM/COADS fluxes but remains consistent with NCEP.

Water in the upper limb of the overturning cell enters the subtropical box through the Straits of Florida (30 Sv; Schott et al. 1988), the Antilles Current east of the Bahamas (19 ± 9 Sv) and via Ekman transport across 24°N (4.3 Sv). Much of this recirculates southward in the subtropical gyre (Fig. 10), leaving a net northward transport of 16.6 ± 1.5 Sv across 24°N ($\gamma^n < 27.74$). Within the subtropical box, outcropping water at $\gamma^n > 24.7$ loses a net 0.40 ± 0.04 PW, concentrated in the Gulf Stream and its recirculation. The associated air–sea transformation reaches a peak of 19.2 ± 3.3 Sv at $\gamma^n = 26.4$, producing an air–sea buoyancy convergence (formation) of 19 Sv in STMW densities (Speer and Tziperman 1990) and downward-plunging streamlines within the subtropical box (Fig. 9). Some of this water reenters the equatorial box in the subtropical gyre where

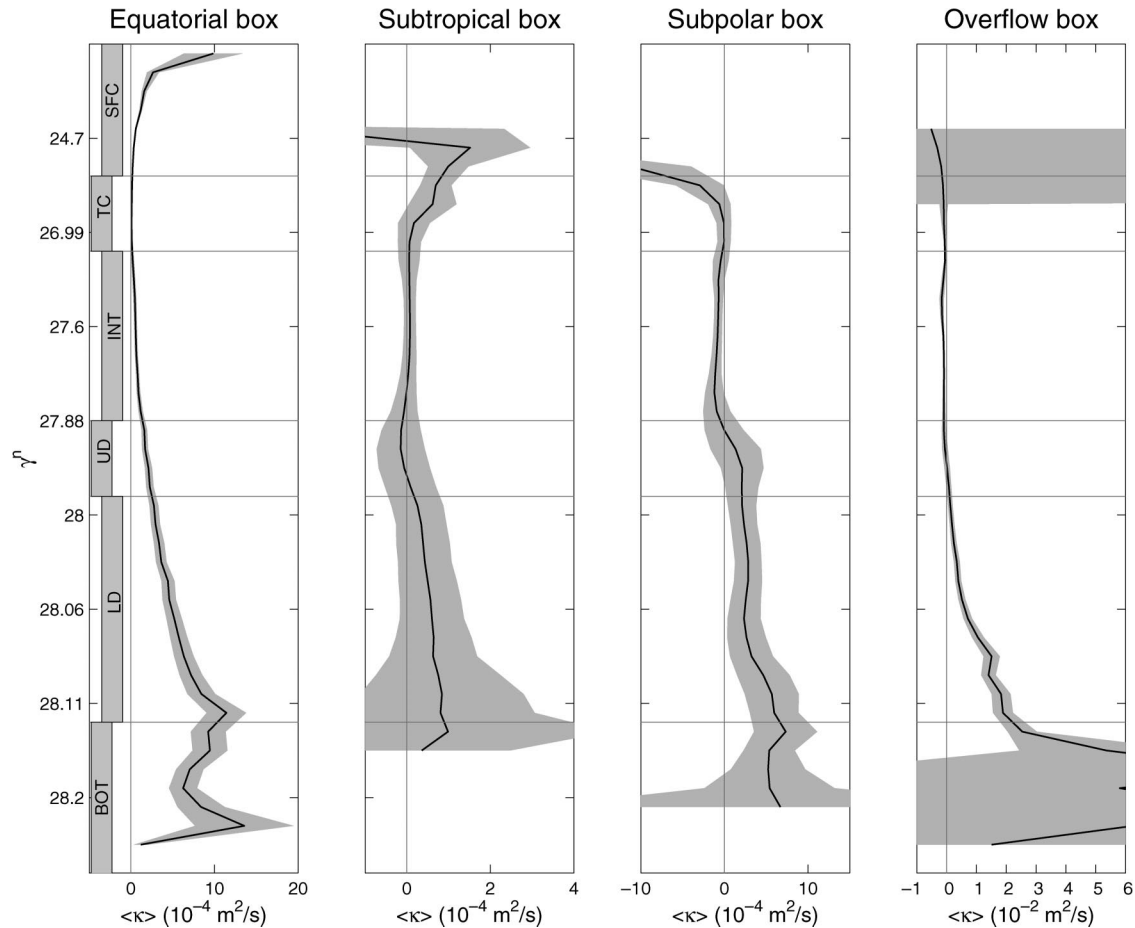


FIG. 7. Effective diapycnal diffusivities (horizontal axes) as a function of neutral density (vertical axes), calculated from the interior mixing component of the diapycnal volume transport A ; shading is standard error.

it is heated, reconverted to surface layers, and returned to the subtropical box, creating a diapycnal signature of this predominantly isopycnal recirculation. The remainder of the STMW continues northward in the Gulf Stream extension and leaves the subtropical box across 48°N . Within the subtropical box, the heat balance of the upper thermocline and surface layers $\gamma^n < 26.72$, which include STMW, is primarily a balance between

advective input through the Straits of Florida (0.58 ± 0.9 PW relative to the mean temperature of the interface $\gamma^n = 26.72$) and loss by advection across 24°N Bahamas to Africa (0.14 ± 0.11 PW), 48°N (0.04 ± 0.04 PW) and loss to the atmosphere (0.36 ± 0.03 PW absolute heat loss). A diffusive or eddy flux of 0.04 ± 0.22 PW across $\gamma^n = 26.72$ (which outcrops in the North Atlantic Current) is needed to close this budget but is not for-

TABLE 3. Vertically integrated transports of volume, heat, and salt across the hydrographic sections in the inverse model solution. “Net GIS” is the combined flux across the Denmark Strait and Iceland–Scotland sections. Positive values are northward (westward for AR16).

Section	Volume (Sv)	Heat (PW)	Salt (10^6 kg s^{-1})
Net GIS	0.1 ± 0.3	0.30 ± 0.03	7 ± 13
AR18 (Denmark Strait)	-4.0 ± 0.7	0.05 ± 0.02	-142 ± 27
Iceland–Scotland	4.1 ± 0.7	0.25 ± 0.02	149 ± 25
AR7E (60°N)	0.1 ± 0.6	0.44 ± 0.03	6 ± 26
AR19 (48°N)	-0.5 ± 1.0	0.60 ± 0.04	-10 ± 36
AR16 (Gulf of Cadiz)	0.0 ± 0.2	-0.04 ± 0.02	0 ± 9
A5 (24°N ; total)	-1.0 ± 1.4	1.17 ± 0.08	-31 ± 50
A5 (Florida Strait)	29.9 ± 1.6	2.42 ± 0.11	1148 ± 34
A5 (Bahamas–Africa)	-30.9 ± 2.1	-1.24 ± 0.10	-1162 ± 48
A8 (11°S)	-0.7 ± 1.2	0.69 ± 0.10	-18 ± 59

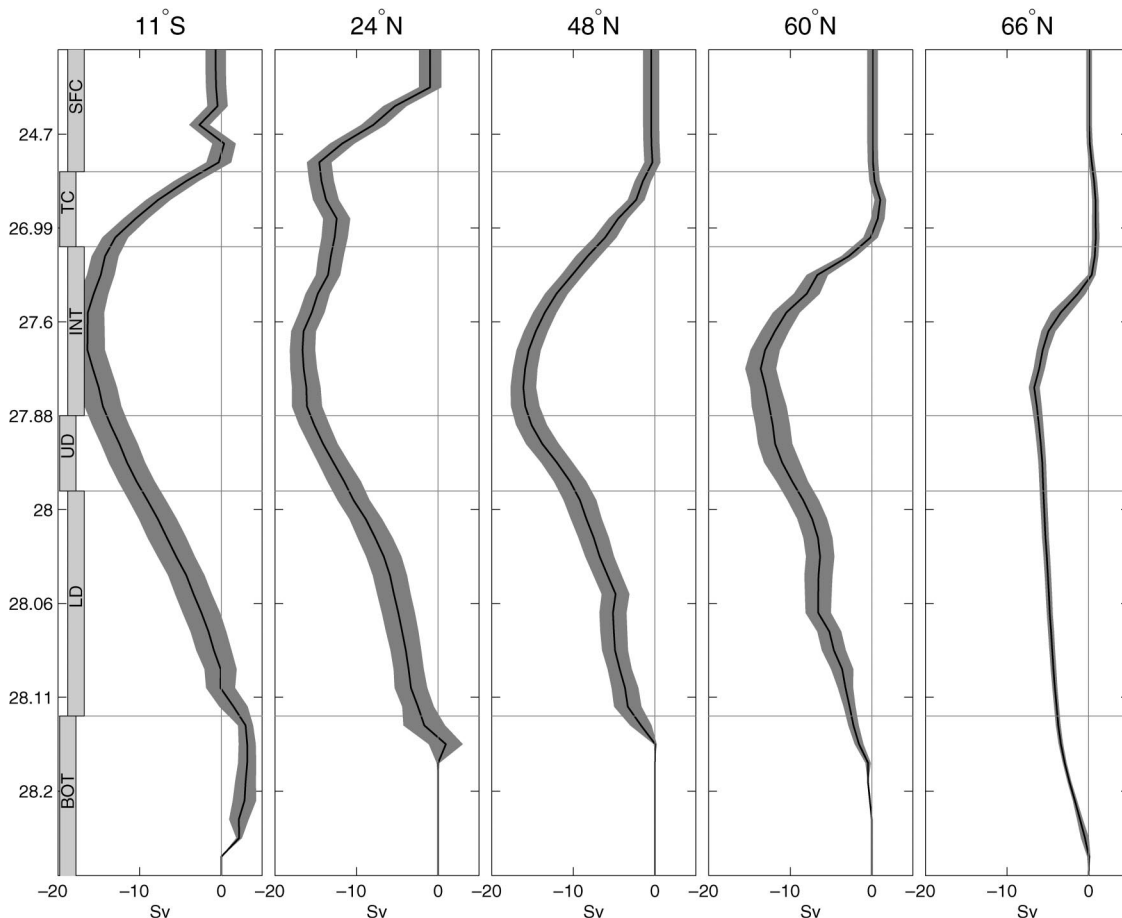


FIG. 8. Overturning streamfunction across hydrographic sections A8 (11°S), A5 (24°N), AR19 (48°N), AR7E (60°N), and the combined GIS ridge sections (66°N). Positive is northward. Standard error bars are indicated by shading.

mally significant. In order to generate the observed characteristics of STMW, a different relative combination of salt and heat diffusion is required: while heat diffusion is negligible in the thermocline layers, salt diffusion transfers $5 \times 10^6 \text{ kg s}^{-1}$ salt out of mode water layers to lower density (Fig. 6), that is, acts to reduce the salinity increase caused by net $E - P$.

Across the Gulf of Cadiz section, $2.2 \pm 0.6 \text{ Sv}$ overturning is associated with the conversion of $\gamma^n < 27.4$ water to the range $27.4 < \gamma^n < 27.96$ within the Mediterranean Sea and Strait of Gibraltar (Baringer and Price 1997). Figure 9 reflects this transformation as an apparent downwelling at dense thermocline to intermediate layers between 24° and 48°N. This transformation is not explicitly resolved in the model domain—in fact, there is no significant mixing in these subsurface layers within the subtropical box (Fig. 6).

Northward flow across 48°N is concentrated in the western Atlantic, on both sides of a strong anticyclonic recirculation in the western boundary (the Mann Eddy; Mann 1967). The net northward transport at 48°N is $16.1 \pm 1.6 \text{ Sv}$ for $\gamma^n < 27.84$. This water enters the subpolar gyre (the combined subpolar and overflow box-

es), where it loses $0.31 \pm 0.03 \text{ PW}$ to the atmosphere. The associated air–sea transformation F_p peaks at $12.6 \pm 1.1 \text{ Sv}$ ($\gamma^n = 27.41$) and drops to zero by $\gamma^n = 28.04$, yielding a formation of 12.6 Sv of SPMW. Of this, $3.1 \pm 1.6 \text{ Sv}$ is at extreme SPMW (e.g., Labrador Sea Water) densities of $\gamma^n > 27.88$ ($\sigma_\theta \approx 27.74$ at 48°N). An additional $5.8 \pm 3.1 \text{ Sv}$ of water is advected to layers denser than $\gamma^n > 27.88$ by interior mixing, representing mixed layer entrainment, eddy stirring across outcropping isopycnals, and warm water entrainment at the overflows; $2.5 \pm 2.3 \text{ Sv}$ continues to densities greater than $\gamma^n = 27.98$ ($\sigma_\theta \approx 27.81$). The resulting mixing-driven advective convergence is the same strength as air–sea formation in the LSW density range ($27.91 < \gamma^n < 27.98$), and the combined formation (air–sea plus mixing) accounts for nearly all of the $5.9 \pm 2.0 \text{ Sv}$, which is exported southward across 48°N in this density range. Subtracting the 0.6 Sv that enters the overflow box over the GIS ridges and interpolating to extract the total formation rate in the range $27.74 < \sigma_\theta < 27.80$ yields a value of $4.7 \pm 2.0 \text{ Sv}$, within the estimates of mean LSW production from CFC inventories in the same σ_θ range (4.4–5.6 Sv; Rhein et al. 2002).

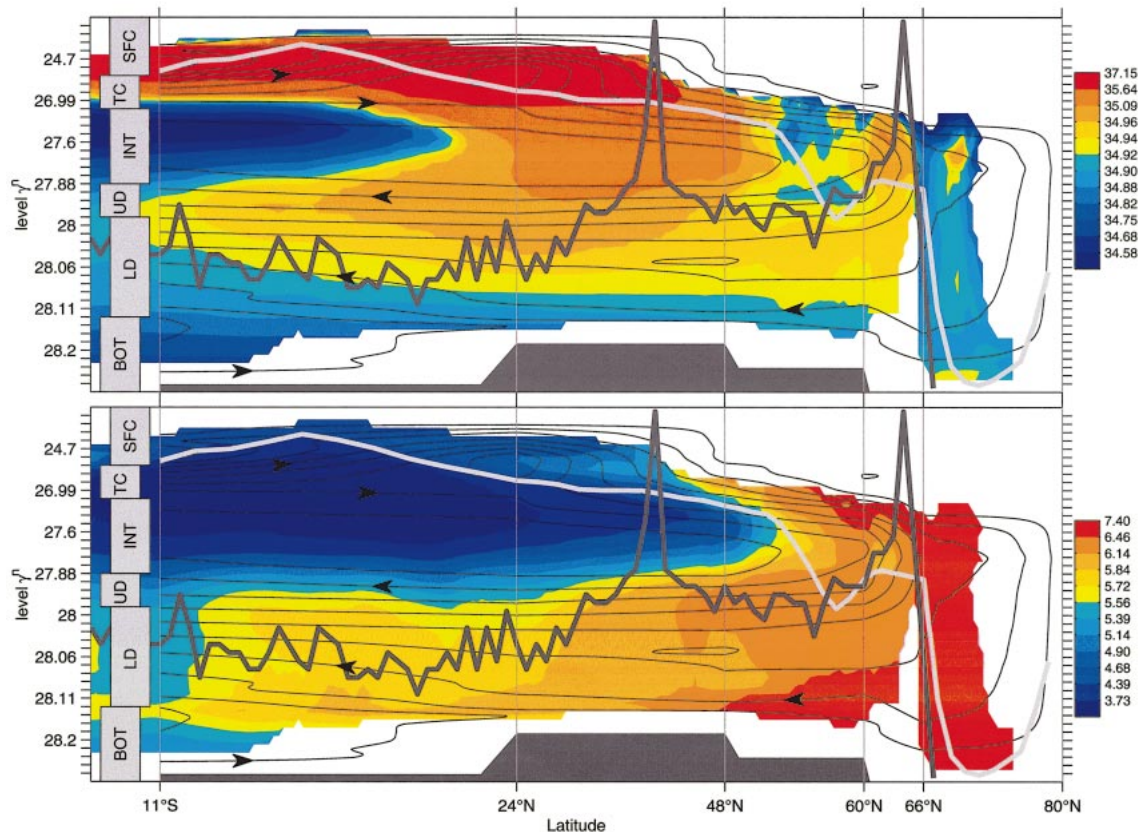


FIG. 9. Side view of the North Atlantic meridional overturning, contoured in 2-Sv intervals, superimposed on zonally averaged (top) salinity and (bottom) oxygen (mL L^{-1}) calculated from climatology (Gouretski and Jancke 1998). Light gray curve: densest outcropping layer, estimated from COADS climatology. Dark gray curve: crest of the Mid-Atlantic Ridge, including the Azores Plateau and Iceland.

A total of 6.5 ± 0.7 Sv Atlantic water at $\gamma^n < 27.79$ leaves the domain across the GIS ridges, via the Irminger and Norwegian Atlantic Currents. Within the GIN Seas, this water is converted to NSOW, which returns to the North Atlantic through channels in the GIS ridges (cf. Mauritzen 1996). The overflow spans a broad range of densities; the densest, 1.6 ± 0.2 Sv at $\gamma^n > 28.12$ through the Faroe Bank Channel and 1.5 ± 0.3 Sv at $\gamma^n > 28.23$ through the Denmark Strait channel, is not present in AR7E (60°N) and therefore must be mixed to lighter layers entirely within the overflow box. At densities $27.6 < \gamma^n < 28.08$ ($27.5 < \sigma_\theta < 27.89$ at 60°N) within the overflow box, interior mixing transforms water to denser layers. The resulting mixing-driven convergence centered on $\gamma^n \approx 28.1$ is a robust result of the inversion (e.g., Fig. 4), consistent with detrainment of the dense overflow and entrainment of less-dense water, in the overflow plumes descending from the mouths of the Denmark Strait and Faroe Bank channels (cf. Speer and Tziperman 1990).

At densities $\gamma^n > 27.96$ ($\sigma_\theta > 27.8$), 13.1 ± 1.7 Sv crosses 60°N in the southward deep boundary current against Cape Farvel, Greenland, consistent with Dickson and Brown (1994). The net outflow across 60°N in

these layers is 9.8 ± 1.9 Sv, fed by 5.6 ± 0.5 Sv overflow across the GIS ridges plus entrainment of 3.0 ± 2.3 Sv from lighter layers. Thus, the model results imply that entrainment is the same size as lateral isopycnal transport in these layers and that entrainment and detrainment within these layers significantly affect the density structure of water exported in the deep boundary current.

5. Conclusions

Using a statistical best-fit method we have estimated large-scale circulation, transports, the distribution of mixing, and air-sea fluxes, which are simultaneously consistent with the North Atlantic hydrography and a wide range of constraints from regional studies. The method handles explicitly the effect of air-sea transformation where layers outcrop. This allows us, for instance, to extend the model beyond 48°N without abandoning resolution of outcropping layers. The result of this added information is to produce better-constrained estimates of property transports.

In the inverse solution, average mixing (Fig. 7) has a well-determined structure related to air-sea transfor-

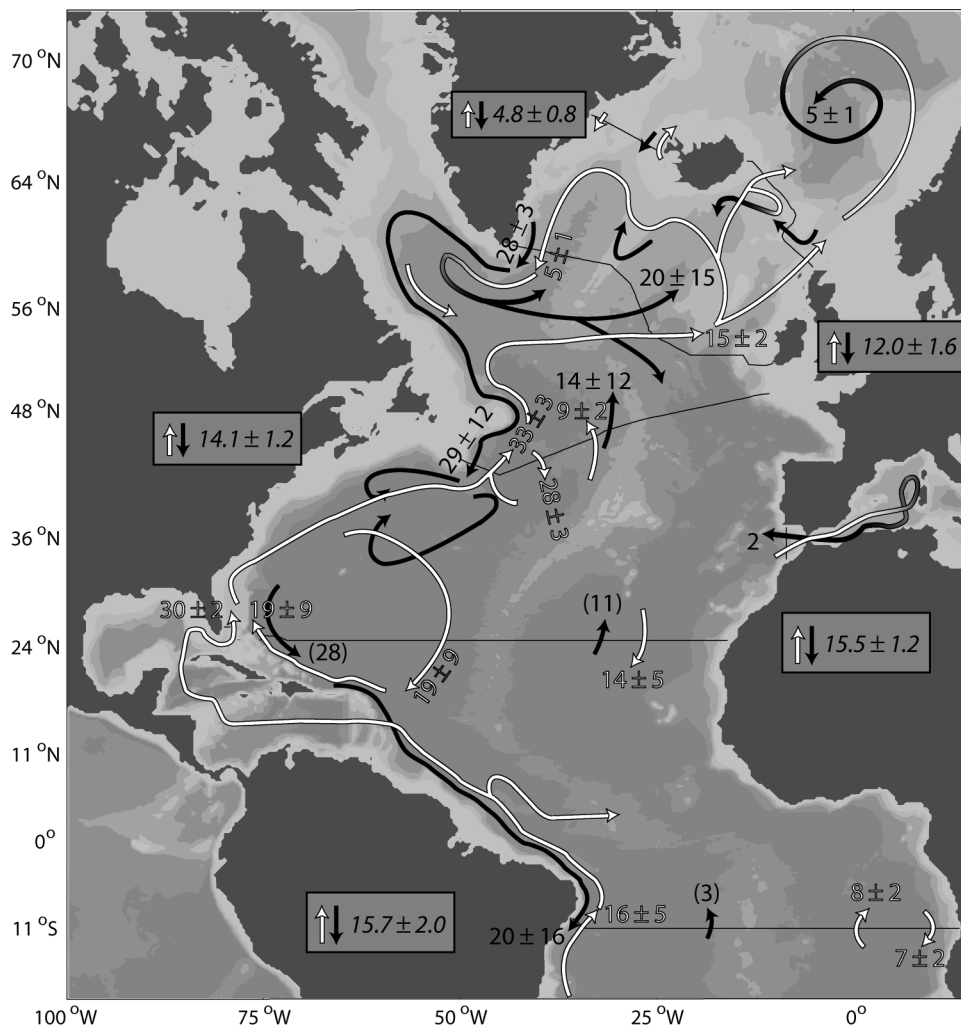


FIG. 10. Circulation of thermocline (white arrows; $\gamma^n < 27.6$) and deep (black arrows; $\gamma^n > 27.6$) water in the inverse solution. Numbers indicate transport (Sv) where currents cross the hydrographic sections; values in parentheses are not well-determined in the solution. The strength of the net overturning exchange between these layers is given in panels; north of 11°S, larger values are found for denser interfaces.

mation, overflow, and deep upwelling. The solution shows two major overturning cells: a thermocline plus intermediate water cell and a dense overflow cell. The overflow component is ~40% of the total. A third, smaller cell is associated with the inflow and upwelling of AABW. All cells ultimately depend on air–sea forcing at the surface, but the overflow presents a strong and distinct control; in the overflow box, vertical and horizontal transports are the same strength, and intense recirculation around the boundary and within the adjacent Irminger and Iceland basins absorbs and transmits overflow water. Hints of a shallow tropical cell are present, and significant diapycnal transports occur in the equatorial box, but we are unable to distinguish mixing at the equator from that occurring elsewhere within the box, and so this aspect of the solution has not been pursued here.

The net isopycnal volume transports across each sec-

tion and diapycnal transports across layer interfaces may be combined to yield bulk volume fluxes into/out of each block of layers in each box. The layers' volume divided by this flux gives a mean residence time, updating Worthington's (1976) values (Table 4; these should not be equated with age, i.e., time since outcropping). The smallest residence time is the ~10 days required to flush bottom layers ($\gamma^n > 28.127$) in the overflow box—this densest overflow is vigorously detrained after flowing through the Faroe Bank Channel and rapidly advected in the deep boundary current from the Denmark Strait channel to Cape Farvel. The largest well-defined residence times are in lower deep layers, which require ~100 years to renew their large volumes within the equatorial and subtropical boxes, and in intermediate layers of the equatorial box, which require ~150 years because they are near the turning density of the overturning circulation. Mean residence times in

TABLE 4. Bulk volume fluxes (\dot{V}), volumes (V), and mean residence times (T_{res} , range of values from the standard error of \dot{V}) for layer blocks (see Table 2).

Box		TC	INT	UD	LD	BOT
Overflow	\dot{V} (Sv):	3.5 ± 0.5	12.7 ± 2.2	6.5 ± 2.2	6.0 ± 2.0	3.7 ± 0.6
	V (10^6 km^3):	0.04	1.61	0.96	0.68	0.003
	T_{res} (yr):	0.3–0.4	3.4–4.9	3.5–7.1	2.7–5.4	0.002–0.031
Subpolar	\dot{V} (Sv):	8.4 ± 1.8	7.4 ± 1.9	6.6 ± 2.2	7.5 ± 2.2	2.2 ± 0.6
	V (10^6 km^3):	0.28	2.55	3.36	4.53	0.28
	T_{res} (yr):	0.87–1.34	8.7–15	12–24	15–27	3.2–5.5
Subtropical	\dot{V} (Sv):	21.2 ± 1.3	6.0 ± 0.7	6.3 ± 2.4	8.7 ± 3.2	1.7 ± 1.3
	V (10^6 km^3):	6.68	10.96	8.63	26.28	2.68
	T_{res} (yr):	9.4–11	52–66	31–70	70–150	28–210
Equatorial	\dot{V} (Sv):	22.3 ± 1.2	4.8 ± 1.5	6.0 ± 2.0	13.2 ± 2.3	4.6 ± 2.7
	V (10^6 km^3):	8.97	23.03	10.22	45.44	5.42
	T_{res} (yr):	13–14	120–220	40–81	93–130	24–90

upper deep layers are 20–50 years throughout most of the North Atlantic.

Acknowledgments. We thank A. Tandon and A. Thurnherr for their input and assistance throughout this project. Author RL thanks the hosts and participants of the 2001 WOCE Young Investigators' Workshop. The inverse model was developed from DOBOX code (Morgan 1995) and generous assistance from B. Sloyan helped us to initiate the study. The study also benefited from communications with C. Wunsch, P. Saunders, C. Mauritzen, and S. Josey. NCEP reanalysis data were provided by the NOAA–CIRES Climate Diagnostics Center (<http://www.cdc.noaa.gov/>). RL and KS received support from NSF grant OCE-9906657.

APPENDIX A

Air–Sea and Land–Sea Fluxes

a. Heat and freshwater

The monthly mean climatologies were the UWM/COADS (da Silva et al. 1994) and the 22 April 2002 version NCEP–NCAR reanalysis products. For each month, sea surface γ^n was calculated from SST and SSS fields (the latter from Levitus and Boyer 1994), and then the net heat and freshwater ($P - E$) fluxes were summed for each outcropping model layer. Accumulation over the 12 months produced an estimate of the annual mean fluxes into each layer. Air–sea transformation F_p was calculated with (4) for each month and accumulated similarly.

b. Rivers

The 60 largest rivers flowing into the Atlantic (total: 0.33 Sv) were extracted from the Global Runoff Data Center database (Grabs et al. 1996). This freshwater input was included in the prior volume and buoyancy budgets by adding each river's transport to the UWM/COADS or NCEP–NCAR grid point closest to the river mouth.

c. Wind stress

Monthly mean wind stresses were used from the NCEP–NCAR reanalysis and from the Southampton Oceanography Centre reanalysis of COADS, which uses a larger drag coefficient than UWM/COADS at high wind speeds to match more closely direct observations (Josey et al. 2002). For each layer the Ekman transport across a section was calculated for the 12 climatological months and assumed to advect monthly temperature and salinity at 10-m depth (Levitus and Boyer 1994).

APPENDIX B

Prior Unknown Variances and Model Errors

Prior variances for the unknowns and model errors were contained in matrices R_{xx} , R_{nn} (cf. Wunsch 1996). In the absence of knowing the full covariance structure of these prior matrices, we took both as diagonal.

Adjustments to reference velocities were required to be in a range $\pm |v_{\text{ref}}|_{\text{ap}}$. Interior (nonboundary) values of $|v_{\text{ref}}|_{\text{ap}}$ were chosen to be section-dependent constants of 1–10 cm s^{-1} (see Table 1), with larger values for sections dominated by shallow flow over sharp bathymetry. In the western boundaries of the 11°S, 24°N, and 48°N sections, $|v_{\text{ref}}|_{\text{ap}}$ was increased to 40 cm s^{-1} to allow strong WBC adjustment. In addition, at each station pair a second value of $|v_{\text{ref}}|_{\text{ap}}$ was calculated to accommodate a ± 250 -dbar uncertainty in the reference level, an error range inferred from analysis of a GCM (Ganachaud 1999). The larger of the two values was used for each pair.

Prior values for the air–sea inputs of heat, freshwater, and momentum were taken as the mean of the COADS- and NCEP-derived calculations. The squared difference between the integrated flux estimates from the two products was used as the permitted variance of the F^* , e^* adjustment. This choice accommodates both COADS and NCEP fields in the prior error.

The interior (subsurface) mixing of density, salt, and heat were given prior values of zero. The allowed variance of the density mixing terms $\partial_\rho D_\rho$ were calculated

from the prior transformation equation for each layer. After some experimentation we added a uniform 2 Sv to the allowed adjustment within each layer in order to achieve a solution with lower overall mixing, potentially at the expense of higher mixing in some individual layers. Variances for the unknown diffusion and eddy transports of heat and salt were calculated similarly, that is, the value needed to satisfy the prior budgets, consistent with our goal of seeking a minimum-mixing solution.

By applying a box inverse model to the output of a forward model, Ganachaud (1999) has shown that net volume conservation should be less strictly imposed than in earlier efforts, primarily due to temporal variations in the upper-ocean baroclinic structure of low-latitude sections. In this study, each section is assigned a net error T_{ap} (see Table 1) due to asynopticity. The prior variance from exact net volume conservation within a box is given by the sum of the T_{ap}^2 for the sections bounding that box. To make an observation-based estimate of individual layer errors due to asynopticity, we calculated the combination of bottom-referenced thermal wind and reference level velocity offset, which yield 31 Sv for the August 1992 and February 1998 WOCE repeats of the Straits of Florida section. Within individual isopycnal layers, the difference in volume transport ranged from 1.2 Sv (lightest layer) to <0.2 Sv for layers denser than $\gamma^n = 25.3$. We used these values as the prior errors on volume conservation within layers, with 0.2 Sv assigned to all layers at $\gamma^n > 25.3$ (layers 7–45, representing 98.9% of the ocean's volume in the study domain). To estimate the model error in heat conservation, we multiplied the layers' volume error by the sum of the box- and layer-dependent mean potential temperature $\langle \theta \rangle$ and twice the standard deviation of θ within the layer, in the bounding hydrographic sections. The second term represents possible correlations between potential temperature anomalies and eddy mass fluxes (Ganachaud 1999). A similar procedure was used for salt anomaly conservation, using the salinity anomaly $(S - 35)/1000$.

APPENDIX C

Hydrographic Sections

For each hydrographic section (Table 1), a thermal wind reference level (isobaric or isopycnal) or set of levels were chosen based on existing literature and net continuity arguments. For some station pairs, nonzero initial reference velocities were included so that the prior velocity field was consistent with additional, section-dependent constraints in particular layers. Often in the literature, net transports are given for a range of σ_θ or θ . We convert σ_θ to γ^n (and thus to model layer number) using the scatter plot of σ_θ versus γ^n for the section. Temperature-defined layer transports were identified by the layer-mean θ - S relation of the section.

a. Canadian Archipelago throughflow

A transport of 0.9 ± 0.2 Sv, $(31 \pm 6) \times 10^6$ kg s⁻¹ salt was added to the mass and salt budgets of the sub-polar box. This volume transport matches the Bering Strait throughflow (0.8 Sv; Coachman and Aagaard 1988) combined with 0.1 Sv net $P + R - E$ and ice melt in the Arctic Ocean. Applying this transport to water in the Canadian Archipelago (mean salinity 33.6 psu in the SAC/Hamburg climatology) gives the corresponding salt transport. The inversion was also required to match the Bering Strait salt transport, $(26.7 \pm 19) \times 10^6$ kg s⁻¹, via the combined southward salt input through the Denmark Strait and Iceland–Scotland sections and the Canadian Archipelago input (Wijffels et al. 1992).

b. Denmark Strait

Thermal wind for WOCE section AR18 was calculated relative to a bottom level of no motion. Without additional information, the model fails to produce an acceptable overflow. The inverse model is “informed” of the bathymetrically controlled flow via additional constraints:

- No net mass transport into GIN Seas: 0 ± 0.35 Sv across the Greenland–Scotland ridges (AR18 and the Iceland–Scotland section), all layers.
- Denmark Strait overflow: 2.0 ± 0.2 Sv southward in layers 38–45 ($\gamma^n > 28.14$) (Girton et al. 2001).
- Denmark Strait overflow: 0.9 ± 0.1 Sv southward, layers 27–37 ($28.01 < \gamma^n < 28.14$) (Girton et al. 2001).
- Polar water in the East Greenland Current: 1.6 ± 0.5 Sv southward, westernmost 15 station pairs, layers 1–15 ($\gamma^n < 27.6$) (Malmberg et al. 1972; Mauritzen 1996).
- Irminger Current branch: 0.9 ± 0.4 Sv northward in easternmost five station pairs, layers 1–15 ($\gamma^n < 27.6$) (Kristmannsson et al. 1989; Mauritzen 1996).

c. Iceland–Scotland Ridge

Because of the complex bathymetry between Iceland and Scotland, an ideal hydrographic section separating the North Atlantic Ocean and the Norwegian Sea would run southeast from Iceland along the Iceland–Faroe Rise to the Faroe Shelf, southwest across the Faroe Bank Channel (FBC) to the Faroe Bank, then southeast along the Wyville–Thompson Ridge to the Hebridian Shelf off the Scottish coast. Unfortunately, no such section exists in the WOCE database. We assembled a composite section from the International Council for the Exploration of the Sea (ICES) Service Hydrographique data base. Three segments, all from the North Atlantic and Norwegian Sea Exchange (NANSEN) experiment, span most of the ideal path but terminate on the Iceland–

Faroe Rise 230 km from the Iceland coast. This gap was filled by a segment from the Variability of Exchanges in the Northern Seas (VEINS) experiment, collected 10 yr after the 1986–88 NANSEN sections. Thermal wind was calculated relative to a level-of-no-motion at $\gamma^n = 27.88$, separating northward-flowing Atlantic water and southward-flowing overflow. Despite the temporal separation between the VEINS and NANSEN segments, they had nearly identical vertical profiles of temperature and salinity where they were joined, producing a maximum thermal wind of 0.5 cm s^{-1} (the near-concurrent pairs on either side have maxima of 1.9 and 5.7 cm s^{-1}). Section-dependent constraints imposed on the inverse solution were:

- Faroe Bank Channel Overflow: $1.4 \pm 0.2 \text{ Sv}$ southward, layers 38–45 ($\gamma^n > 28.14$) (Saunders 1990; Mauritzen 1996; Østerhus et al. 1999; Price et al. 2001).
- Overflow across Iceland–Faroe Rise (including North Icelandic Winter Water and Arctic Intermediate Water): $0.85 \pm 0.3 \text{ Sv}$ southward, westernmost 14 station pairs, layers 21–45 ($\gamma^n > 27.88$) (Saunders 1990; Mauritzen 1996).
- Atlantic water across Iceland–Faroe Rise: $4.0 \pm 0.4 \text{ Sv}$ northward, westernmost 14 station pairs, layers 1–20 ($\gamma^n < 27.88$) (Hansen et al. 1999).
- Norwegian Atlantic Current between Faroe Islands and Scotland: $3.0 \pm 0.4 \text{ Sv}$ northward, easternmost 18 station pairs, layers 1–20 ($\gamma^n < 27.88$) (Gould et al. 1985; Mauritzen 1996; Hansen et al. 1999).

d. Greenland to Ireland, 60°N

The second repeat of WOCE line AR7E/A1E (1992) ran from Cape Farvel, Greenland, to the Porcupine Bank, west of Ireland, passing over the Reykjanes Ridge approximately halfway between Iceland and the Charlie Gibbs Fracture Zone and also passing close to the southern edge of the Rockall Plateau. Ice conditions against the Greenland coast were favorable during this cruise, allowing water in the East Greenland Current (EGC) to be sampled to 38 km offshore. The eastern end of AR7E lies on the Porcupine Bank (an extension of the Hebridian Shelf) at a depth of 320 m, but still 240 km from the Irish coast. Thus, while northward-flowing Atlantic water is sampled in this section, an area of potentially significant transport over the shelf is missed. This gap was filled with a segment of the previous year's AR7E repeat, which began 60 km west of the Irish coast but had encountered ice 45 km farther offshore of Greenland. Water properties on the Porcupine Bank had not changed significantly between 1991 and 1992: at their closest casts, salinity and temperature have smaller differences than similarly spaced 1992 casts farther west on the bank. Thermal wind was calculated relative to $\gamma^n = 27.88$. Section-dependent constraints imposed on the inverse solution were:

- EGC, Greenland to 2000-m isobath: $15 \pm 2 \text{ Sv}$ southward, westernmost five station pairs, all layers (Bacon 1997).
- Total EGC strength: $32.2 \pm 3.2 \text{ Sv}$ southward, westernmost seven station pairs, all layers (Bersch 1995).

e. North America to Europe, 48°N

Thermal wind was calculated relative to the no-motion level $\gamma^n = 27.88$. No section-dependent constraints were imposed.

f. Gulf of Cadiz

Thermal wind was calculated relative to a bottom reference level. Section-dependent constraints were:

- No net transport across section: $0 \pm 0.25 \text{ Sv}$, all layers.
- Mediterranean Water outflow: $2.0 \pm 0.5 \text{ Sv}$ westward, layers 15–20 ($27.52 < \gamma^n < 27.88$) (Baringer and Price 1997).
- No net flow at densities greater than North Atlantic Central Water: $0 \pm 0.125 \text{ Sv}$, layers 23–45 ($\gamma^n > 27.94$).

g. North America to Europe, 24°N

For the Straits of Florida segment of this section, thermal wind was calculated relative to a northward 28.5 cm s^{-1} at the bottom, producing a prior transport of 31 Sv. For the rest of the section (Bahamas to Africa), thermal wind was calculated relative to an isobaric level of no motion at 3000 dbar (Rintoul and Wunsch 1991). The inverse model was constrained to retain a net transport of $31 \pm 2 \text{ Sv}$ northward in the Straits of Florida (Schott et al. 1988).

h. South America to Africa, 11°S

Thermal wind was calculated relative to the isobaric reference levels of Speer et al. (1996): 1100 m in the western boundary (west of 35.5°W), 3800 m in the Brazil Basin ($17.67^\circ\text{--}35.5^\circ\text{W}$), 2400 m over the Mid-Atlantic Ridge ($10.17^\circ\text{--}17.67^\circ\text{W}$), and 4000 m in the Angola Basin (east of 10.17°W). Section-dependent constraints were:

- Bering Strait volume transport minus integrated North Atlantic $E - P - R$ across 11°S : $0.58 \pm 2.0 \text{ Sv}$ southward, all layers.
- Bering Strait salt flux across 11°S : $(26.7 \pm 72.9) \times 10^6 \text{ kg s}^{-1}$ salt southward, all layers.
- Antarctic Bottom Water, supplying $2.14 \pm 1 \text{ Sv}$ into the Guiana Basin (Hall et al. 1997) and $1.22 \pm 0.25 \text{ Sv}$ through the Romanche and Chain Fracture Zones (Mercier and Speer 1998): $3.4 \pm 1 \text{ Sv}$ northward, layers 37–45 ($\gamma^n > 28.12$).

- No net flow of lower deep water east of the Mid-Atlantic Ridge: 0 ± 2 Sv, pairs 57–109, layers 35–45 ($\gamma^{\sigma_t} > 28.10$).

REFERENCES

- Bacon, S., 1997: Circulation and fluxes in the North Atlantic between Greenland and Ireland. *J. Phys. Oceanogr.*, **27**, 1420–1435.
- , 1998: Decadal variability in the outflow from the Nordic seas to the deep Atlantic Ocean. *Nature*, **394**, 871–874.
- Baringer, M. O., and J. F. Price, 1997: Mixing and spreading of the Mediterranean outflow. *J. Phys. Oceanogr.*, **27**, 1654–1692.
- Bersch, M., 1995: On the circulation of the northeastern North Atlantic. *Deep-Sea Res.*, **42A**, 1583–1607.
- , J. Meincke, and A. Sy, 1999: Interannual thermohaline changes in the northern North Atlantic 1991–1996. *Deep-Sea Res.*, **46B**, 55–75.
- Coachman, L., and K. Aagaard, 1988: Transports through Bering Strait: Annual and interannual variability. *J. Geophys. Res.*, **93**, 15 535–15 539.
- da Silva, A. M., C. C. Young, and S. Levitus, 1994: *Algorithms and Procedures. Atlas of Surface Marine Data 1994*. Vol. 1. NOAA Atlas NESDIS 1, 51 pp.
- Dickson, R. R., and J. Brown, 1994: The production of North Atlantic Deep Water: Sources, rates, and pathways. *J. Geophys. Res.*, **99**, 12 319–12 341.
- Ganachaud, A. S., 1999: Large scale oceanic circulation and fluxes of freshwater, heat, nutrients and oxygen. Ph.D. thesis, MIT–WHOI Joint Program, 249 pp.
- , and C. Wunsch, 2000: Improved estimates of global ocean circulation, heat transport and mixing from hydrographic data. *Nature*, **408**, 453–457.
- Girton, J. B., T. B. Sanford, and R. H. Käse, 2001: Synoptic sections of the Denmark Strait Overflow. *Geophys. Res. Lett.*, **28**, 1619–1622.
- Gould, W. J., L. Loynes, and J. Backhaus, 1985: Seasonality in slope current transports N. W. of Shetland. *ICES CM*, **C:7**, 1–13.
- Gouretski, V., and K. Jancke, 1998: A new World Ocean climatology: Optimal interpolation of historical and WOCE hydrographic data on neutral surfaces. WOCE Rep. 162/98. [Available from WOCE Special Analysis Center, Max Planck Institute, Hamburg, Germany.]
- Grabs, W., T. de Couet, and J. Pauler, 1996: Freshwater fluxes from continents into the world oceans based on data of the Global Runoff Data Base. Global Runoff Data Centre Tech Rep. 10, Koblenz, Germany, 49 pp.
- Hall, M. M., M. McCartney, and J. A. Whitehead, 1997: Antarctic Bottom Water flux in the equatorial western Atlantic. *J. Phys. Oceanogr.*, **27**, 1903–1926.
- Hansen, B., K. M. H. Larsen, S. Osterhus, B. Turrell, and S. Jónsson, 1999: The Atlantic Water Inflow to the Nordic Seas. *Int. WOCE Newsl.*, **35**, 33–35.
- Jackett, D. R., and T. J. McDougall, 1997: A neutral density variable for the world's oceans. *J. Phys. Oceanogr.*, **27**, 237–263.
- Josey, S. A., E. C. Kent, and P. K. Taylor, 2002: On the wind stress forcing of the ocean in the SOC climatology: Comparisons with the NCEP–NCAR, ECMWF, UWM/COADS and Hellerman and Rosenstein datasets. *J. Phys. Oceanogr.*, **32**, 1993–2019.
- Koltermann, P., A. Sokov, V. Tereschenkov, S. Dobroliubov, K. Lorbacher, and A. Sy, 1999: Decadal changes in the thermohaline circulation of the North Atlantic. *Deep-Sea Res.*, **46B**, 109–138.
- Kristmannsson, S. S., S.-A. Malmberg, and J. Briem, 1989: Inflow of warm Atlantic water to the sub-Arctic Iceland Sea. *Rapp. Pv Réunion. Cons. Int. Explor. Mer*, **188**, 74.
- Large, W. G., and A. J. Nurser, 2001: Ocean surface water mass transformation. *Ocean Circulation and Climate*, G. Siedler et al., Eds., International Geophysics Series, Vol. 77, Academic Press, 317–336.
- Levitus, S., and T. Boyer, 1994: *Temperature*. Vol. 4, *World Ocean Atlas 1994*, NOAA Atlas NESDIS 4, 117 pp.
- Macdonald, A. M., 1998: The global ocean circulation: A hydrographic estimate and regional analysis. *Progress in Oceanography*, Vol. 41, Pergamon, 281–382.
- Malmberg, S. A., H. G. Gade, and H. E. Sweers, 1972: Current velocities and volume transports in the East Greenland Current off Cape Nordenskjöld in August–September 1965. *Proc. Int. Sea Ice Conf.*, Reykjavik, Iceland, 130–139.
- Mann, C. R., 1967: The termination of the Gulf Stream and the beginning of the North Atlantic Current. *Deep-Sea Res.*, **14**, 337–359.
- Marsh, R., 2000: Recent variability of the North Atlantic thermohaline circulation inferred from surface heat and freshwater fluxes. *J. Climate*, **13**, 3239–3260.
- Mauritzen, C., 1996: Production of dense overflow waters feeding the North Atlantic across the Greenland–Scotland Ridge. *Deep-Sea Res.*, **43A**, 769–835.
- McCartney, M. S., 1992: Recirculating components to the deep boundary current of the northern North Atlantic. *Progress in Oceanography*, Vol. 29, Pergamon, 283–383.
- , and L. D. Talley, 1982: The subpolar mode water of the North Atlantic Ocean. *J. Phys. Oceanogr.*, **12**, 1169–1188.
- Mercier, H., and K. G. Speer, 1998: Transport of bottom water in the Romanche Fracture Zone and the Chain Fracture Zone. *J. Phys. Oceanogr.*, **28**, 779–790.
- Morgan, P. P., 1995: Box inverse modelling with DOBOX 4.2. CSIRO Marine Laboratories, Rep. 225, 26 pp.
- Niiler, P. P., and J. Stevenson, 1982: The heat budget of tropical ocean warm-water pools. *J. Mar. Res.*, **40** (suppl.), 465–480.
- Orsi, A. H., W. J. Smethie, and J. L. Bullister, 2002: On the total input of Antarctic waters to the deep ocean: A preliminary estimate from chlorofluorocarbon measurements. *J. Geophys. Res.*, **107** (C8), 31–31-14.
- Østerhus, S., B. Hansen, R. Kristiansen, and P. Lundberg, 1999: The overflow through the Faroe Bank Channel. *Int. WOCE Newsl.*, **35**, 35–37.
- Price, J., T. Sanford, C. Mauritzen, and M. Prater, cited 2001: A report of XCP and CTD data taken during June, 2001, RRS Discovery cruise 247B: A process study of the Faroe Bank Channel overflow. [Available online at <http://www.whoi.edu/science/PO/people/jprice/oflow/FBC.pdf>.]
- Rhein, M., and Coauthors, 2002: Labrador Sea Water: Pathways, CFC-inventory and formation rates. *J. Phys. Oceanogr.*, **32**, 648–665.
- Rintoul, S. R., and C. Wunsch, 1991: Mass, heat, oxygen and nutrient fluxes and budgets in the North Atlantic Ocean. *Deep-Sea Res.*, **38** (suppl.), S355–S377.
- Roemmich, D., and C. Wunsch, 1985: Two transatlantic sections: Meridional circulation and heat flux in the subtropical North Atlantic Ocean. *Deep-Sea Res.*, **32**, 619–664.
- Ross, C. K., 1984: Temperature–salinity characteristics of the “overflow” water in Denmark Strait during “OVERFLOW ‘73”’. *ICES Marine Science Symp.: Hydrobiological Variability in the North Atlantic and Adjacent Seas*, **185**, 111–119.
- Saunders, P. M., 1990: Cold outflow from the Faroe Bank Channel. *J. Phys. Oceanogr.*, **20**, 29–43.
- Schmitt, R. W., P. S. Bogden, and C. E. Dorman, 1989: Evaporation minus precipitation and density fluxes for the North Atlantic. *J. Phys. Oceanogr.*, **19**, 1208–1221.
- Schmitz, W. J., and M. S. McCartney, 1993: On the North Atlantic circulation. *Rev. Geophys.*, **31**, 29–49.
- Schott, F. A., T. N. Lee, and R. Zantopp, 1988: Variability of structure and transport of the Florida Current in the period range of days to seasonal. *J. Phys. Oceanogr.*, **18**, 1209–1230.
- Sloyan, B. M., and S. R. Rintoul, 2001: The Southern Ocean limb of the global deep overturning circulation. *J. Phys. Oceanogr.*, **31**, 143–173.
- Smethie, W. M., D. W. Chipman, J. H. Swift, and K. P. Koltermann, 2000: Chlorofluoromethanes in the Arctic Mediterranean Seas:

- Evidence for formation of bottom water in the Eurasian Basin and deep-water exchange through Fram Strait. *Deep-Sea Res.*, **35A**, 347–369.
- Speer, K. G., 1997: A note on average cross-isopycnal mixing in the North Atlantic Ocean. *Deep-Sea Res.*, **44**, 1981–1990.
- , and E. Tziperman, 1990: Convection from a source in an ocean basin. *Deep-Sea Res.*, **37**, 431–446.
- , J. Holfort, T. Reynaud, and G. Siedler, 1996: South Atlantic heat transport at 11°S. *The South Atlantic: Present and Past Circulation*, G. Wefer et al., Eds., Springer-Verlag, 105–120.
- Walín, G., 1982: On the relation between sea-surface heat flow and thermal circulation in the ocean. *Tellus*, **34**, 187–195.
- Wijffels, S. E., R. W. Schmitt, H. L. Bryden, and A. Stigebrandt, 1992: Transport of freshwater by the oceans. *J. Phys. Oceanogr.*, **22**, 155–162.
- Worthington, L. V., 1976: On the North Atlantic circulation. Johns Hopkins Oceanographic Studies 6, Woods Hole Oceanographic Institution, Rep. 6, 110 pp.
- Wunsch, C., 1984: An eclectic Atlantic Ocean circulation model. Part I: The meridional flux of heat. *J. Phys. Oceanogr.*, **14**, 1712–1733.
- , 1996: *The Ocean Circulation Inverse Problem*. Cambridge University Press, 442 pp.
- , and B. Grant, 1982: Towards the general circulation of the North Atlantic Ocean. *Progress in Oceanography*, Vol. 11, Pergamon, 1–59.